Polymer 51 (2010) 3225–3229

Contents lists available at ScienceDirect

Polymer

journal homepage: www.elsevier.com/locate/polymer

Refractive index crossover and the phase diagram of an iPP/PEOc blend

Yonghua Yao, Xia Dong*, Chenggui Zhang, Fasheng Zou, Charles C. Han*

Beijing National Laboratory for Molecular Sciences, State Key Laboratory of Polymer Physics and Chemistry, Joint Laboratory of Polymer Science and Materials, Institute of Chemistry, Chinese Academy of Sciences, Beijing 100190, China

ARTICLE INFO

Article history:
Received 21 February 2010
Received in revised form
11 May 2010
Accepted 15 May 2010
Available online 24 May 2010

Keywords:
iPP/PEOc blend
Refractive index
Phase diagram

ABSTRACT

The phase diagram of an isotactic polypropylene/poly(ethylene-octene) copolymer (iPP/PEOc) blend system was investigated using phase contrast optical microscopy, laser light scattering and differential scanning calorimetry (DSC). The sample goes through immiscible (opaque) region to transparent region (seemingly miscible) and back to immiscible (opaque) again as temperature increases through 300 °C region. But it turns out that this is not a real one phase region. It is caused by a temperature dependent inversion of refractive indices between the two component polymers, which can be easily misinterpreted as a miscible region between an upper critical solution temperature (UCST) state and a lower critical solution temperature (LCST) state. With a proper interpretation and analysis of this refractive index inversion, the UCST phase diagram of this iPP/PEOc blend system has been obtained.

1. Introduction

Polyolefin is the most widely used polymer material in our daily life. Among all the polyolefins, the isotactic polypropylene (iPP) and its blends/alloys have drawn a lot of attentions in the last few years because of their easy processibility, good thermal and mechanical properties, chemical and moisture resistance, low density and very competitive price which have made them candidates to replace many more expensive and harder to recycle engineering plastics such as ABS, polyurethane, PC/ABS blends, and etc. However, the relatively poor low-temperature fracture characteristics and dimensional stability (due to its high glass transition temperature and relatively high degree of crystallizability) are significant drawbacks for the neat iPP in applications. Therefore, iPP is often blended or alloyed with various elastomeric polyolefins in order to improve the impact strength at low-temperatures. Owing to the very low interfacial tension between the two components, α-olefin copolymers gave competitive edge as the impact modifiers of iPP [1–7].

As we all know, the size distribution and the connectivity of the dispersed (elastomeric) phase are crucial for the final impact resistance of iPP/elastomer blends [8], which, in turn, are affected greatly by the miscibility or compatibility in the molten state [9,10].

In this study, the iPP/PEOc blend system has been studied. Due to the similarity in all the basic chemical units of polyolefin (CH, CH_2, CH_3), the refractive indices of all polyolefin at molten state are quite similar, this makes it very difficult to identify phase boundaries with the traditional optical techniques. On top of that, there are many controversies in the phase behavior of iPP/PEOc blends. PEOc has been reported to be miscible with iPP and even can be treated as a polymeric solvent of iPP [11], while scanning electron microscopy observations and evidence from dynamic mechanical thermal analysis in other report pointed out that iPP and PEOc only partially miscible for blends which have wt.5% ~ wt.10% or less of PEOc [12,13]. Even more, there is no complete phase diagram or in-situ phase separation study reported, which may be caused by the difficulties and conflicts described above.

With phase contrast optical microscopy and light scattering as on-line/in-situ technique, we found a totally optical transparent state at temperature around 300 °C range for this iPP/PEOc blend system, which was generally treated as the indication of a homogeneous or miscible state. However phase separated morphology was found with subsequent temperature increase or decrease. Unlike the duo UCST and LCST type phase behavior of PS/poly(*n*-pentyl methacrylate) or poly(ethylene-co-styrene)/poly(ethylene-co-styrene) systems [14–16], further study revealed that such phenomena for iPP/PEOc was not caused by the existence of a miscible region at around 300 °C but caused by the inversion (or crossover) of the refractive indices between iPP and PEOc. This phenomenon could have misled the interpretation of blends miscibility and added difficulty to determine the phase boundary. Therefore, we think our current study is fundamentally important in order to provide a correct phase diagram for polyolefin blends in general and for iPP/PEOc in specific.

* Corresponding authors. Tel.: +86 10 82612841; fax: +86 10 62521519.
E-mail addresses: xiadong@iccas.ac.cn (X. Dong), c.c.han@iccas.ac.cn (C.C. Han).

0032-3861/$ – see front matter © 2010 Elsevier Ltd. All rights reserved.
doi:10.1016/j.polymer.2010.05.027

2. Experimental section

2.1. Material and blend preparation

The isotactic polypropylene was provided by Yanshan Petrochemical Corp. Inc. with a weight-average molecular weights $M_w = 4.1 \times 10^5$ and a polydispersity index $M_w/M_n = 4.1$. While the poly(ethylene-octene) copolymer was provided by the Dupont-Dow Chemical Company with the $M_w = 1.5 \times 10^5$ and $M_w/M_n = 2.0$. The melting point of iPP and PEOc was 162.2 °C and 53.7 °C separately. The thermal degradation happened beginning from 377 °C to 448 °C separately of iPP and PEOc.

iPP/PEOc Blends with different compositions were prepared by dissolving the two polymers in xylene at 130 °C (approximately 2–3 wt% of total polymer) and stirred thoroughly in sealed tube for about 8 h and then coprecipitated in cooled methanol (at about 0 °C). After filtering, the obtained blends were washed with clean methanol to remove xylene and then dried in air for 24 h. Subsequently, the samples were further dried in a vacuum oven at room temperature for 72 h. The blend is labeled as W*x*, where *x* is the mass percent of iPP in the blend and $x = 2.6, 5, 7.4, 10, 15.1, 50, 89.8, 95, 97.1$ separately in this study.

2.2. Instruments and experiment design

The molecular weight was measured with Waters alliance GPC 2000.

The melting point was measured by Differential Scanning Calorimetry (Mettler DSC 822e). DSC measurements also have been designed to confirm the phase separation in this work.

The thermal degradation temperature was measured with a TGA-7 (A Perkin–Elmer thermal gravimetric analyzer, USA.) in nitrogen atmosphere at the rate of 10 °C/min to determine the upper-limit of experimental temperature range. The results were used to limit our experimental temperature to be lower than the measured degradation temperatures.

A high performance phase contrast optical microscopy (Nikon E600 POL) was used for the optical microscopy measurement of the phase separated structure due to the very small difference in refractive indices between the two components.

The light scattering instrument is constructed in our laboratory [18] and we numerically integrated scattered light within ±30° angle around the set angle of a 2d-detector to determine the cloud points of blends. Refractive index as a function of temperature was measured by using an apparatus constructed based on the refraction principle [17] which has a thermal stability of about ±0.1 °C. After the solution (wt.1% of polymer) and pure solvent (diphenyl ether) were injected into the sector-cells separately, the transmitted laser light is imaged to the position-sensitive detector by a lens in a 2 foci–2 foci configuration. Then the refractive indices of solutions can be measured with a resolution of 10^{-6} RI units [17].

A Linkam LTS 350 hot stage under nitrogen atmosphere was used to control the temperature (Linkam Scientific Instruments Ltd., UK) for microscopy and light scattering measurements.

3. Results and discussion

To study the phase-transition temperature, a step heating method was adopted. The coprecipitated samples were first jumped to a desired temperature and kept for some time. If the phase separation at this specific temperature was observed by using a phase contrast microscopy, we repeated the procedure again by jumping to an even higher temperature until we find the one phase region (we are anticipating an UCST phase behavior first). Then we use light scattering to confirm and determine the cloud point more precisely. This was done by first take the sample to the one phase region and then the temperature was either increased or decreased at constant rate. The plot of integrated intensity of scattered light versus temperature can be used to determine the cloud point.

When we started our study with a W50.0 composition, we found an optically clear one phase region by step increase temperature method described above. However a phase separated pattern became visible either by increasing or by decreasing the temperature from this optically homogeneous temperature, which generally led to the conclusion that the blend exhibits both UCST and LCST behavior.

However, if we choose concentrations with high or low iPP content, the situation seems very different. For example: A typical temperature vs. integrated scattering intensity experiment is shown in Fig. 1 (a) for the W5.0 sample at different cooling rate. The intensity crossover temperature point at different cooling rate is plotted against the cooling rate. The cloud point is defined as the extrapolated temperature to the zero cooling rate as usual. In Fig. 1b and c, this cloud points vs. cooling rates are displayed for this W5.0 sample and also the W15.1 sample.

When the above measurements were repeated for samples of iPP compositions between W15 and W85, the phase diagram obtained does not seem to be correct and cannot be explained with the widely accepted theory of phase separation [19–27] as described in the following:

1. The phase boundary at the top of this UCST curve obtained by the above procedure seems to be too flat.
2. When we decrease or increase temperature from already phase separated region to the visually homogeneous region, the speed of the phase separated blend structure seems dissolving and become transparent too fast. Also the well-coarsened and phase separated morphology immediately appealed after the temperature is increased or decreased from this optically homogeneous region again. It is inconceivable that we could have a super fast mixing/demixing system.
3. When we increased temperature from already phase separated region through the visually homogeneous region, a close similarity between the observed lower temperature structures in the lower temperature side of the UCST and higher temperature structures in the higher temperature side of the apparent LCST was observed except that an opposite contrast (dark region becomes bright and bright region becomes dark) was observed.

From the above results, we questioned the existence of both UCST and LCST behavior for the iPP/PEOc blend. We suspect that this inversion of morphological behavior may be caused by an inversion of refractive index between iPP and PEOc, which resulted to this apparent miscible region at temperatures around 300 °C.

First, DSC was adopted to verify whether phase separation actually happened in the transparent region. The melting behavior of blends under two different thermal history was compared. One was to keep the sample in DSC oven at 200 °C for 60 min to make sure the sample was well phase separated, and the other was to keep the blend at the transparent temperature (310 °C) for 60 min, and then both samples were quenched into liquid nitrogen to “freeze” the possible structure. Then both samples were heated to melt at the rate of 20 °C/min to compare the melting behaviors. The melting peaks of iPP crystalline structure in the two phase separated phases should shift to temperatures close to each other if the sample were actually annealed in a miscible region at 310 °C. Then we should observe very different melting curves for this 310 °C annealed sample from the 200 °C annealed sample which is annealed in a two phase region. However, we observed only

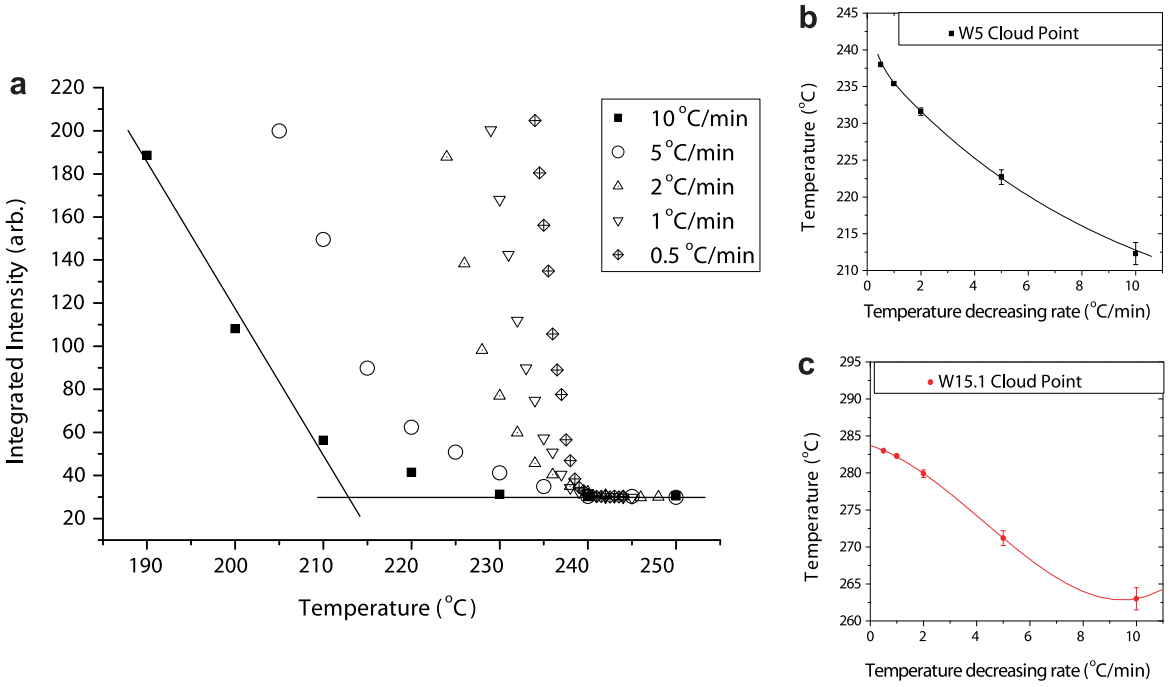

Fig. 1. (a) Plots of integrated scattered intensity measured at different cooling rate versus temperature are shown, in which the W5.0 sample was used. The apparent cloud point obtained from the intersection of integrated scattered intensity change is plotted versus temperature cooling rate were shown as (b) (sample W5.0) and (c) (sample W15.1).

negligible difference, which demonstrated the intrinsically two phase nature at both 200 °C and 310 °C for the iPP/PEOc blends.

Also we raised the temperature of a phase separated sample from 220 °C to 340 °C and take micrographs at the same luminance and white balance conditions every 20 °C. Then we used Scion Image (developed from the NIH image software) program which provides a quantitative intensity of each phase. The two intensities corresponding to the two phases clearly denoted a crossover of the refractive index. Fig. 2 showed an example of such analysis of the W50.0 blend, where refractive index of each phases crossed at about 306 °C. It was revealed that W50.0 sample reached a transparent state (almost the same refractive index for the two components at visible light wave range) around 306 °C, where structures cannot be distinguished by optical methods. And this contrast can be reproduced through the repeating of the thermal history, which verified the existence of such inversion of refractive index. Also, it should be noticed that in Fig. 2a the 200 °C image is almost the same as the 340 °C image except the inversion of the bright and dark phases, and a slight coarsening happened to the sample and resulted in a slight larger domains in the 340 °C images.

Up to this point, we can conclude that the iPP/PEOc system belong to UCST type and exhibits interesting refractive indices crossover behavior which give visually a transparent region and possibly a misleading UCST and LCST behavior.

To further demonstrate our conclusion, we measured the temperature dependence of refractive indices of the two polymers. The refractive indices of polymers were measured in a 1 wt% solution with diphenyl ether (boiling point 258 °C) as the solvent in a sector cell *dn*/*dc* apparatus. Because the voltage output is proportional to the refractive indices difference from the solutions and solvent in the sector cell with our home made refraction index measurement instrument, the temperature dependence of refraction index change is exhibition by temperature dependence of voltage output. Fig. 3 showed the experimental voltage change of the position-sensitive detector, which is related to the $\Delta n/\Delta c$ between the two sectors cells at any given temperature. It is clear that a crossover should happen at around 300 °C with extrapolation.

Lorenz–Lorentz equation may be used to evaluate refractive indices of polymers [28], although normally is used for the amorphous polymers. But in this case, we are only looking at experimental temperatures well above the melting point of both polymers in solutions. In this expression, polarizability, *P*, can be related to the refractive index *n* as:

$$\left(n^2-1\right)\Big/\left(n^2+2\right) = 4\pi P/3 \tag{1}$$

and

$$P = N\alpha \tag{2}$$

Where, *n* is the refractive index, *N* is the molecular number of unit volume, which is related to density ρ. The dipolar polarizability α, is associated to molecular structure.

When combined with Debye formula, a universal refractive index expression can be obtained in the following manner, which demonstrated the relationship with the molecular weight M_W and Temperature *T*.

$$n^2+2 = \frac{3}{1-\frac{4\pi\alpha\rho N_A}{3M_W}} = \frac{3}{1-\frac{4\pi\rho N_A\left[(\alpha_e+\alpha_a)+\frac{\mu_e^2}{3kT}\right]}{3M_W}} \tag{3}$$

where N_A is the Avogadro's number, α_e is the electronic polarizability, α_a is the atomic polarizability, and μ_e is the effective dipole moment. The refractive index *n* changed with two coefficients: the molecular weight M_W and temperature *T*.

Solid lines in Fig. 3 were fitting curves of experimental data based on Equation (3). The refractive index is decreasing with the increasing of temperature for both polymers. iPP has a smaller decreasing rate of refractive index with the increase of temperature compare to the PEOc. This smaller decreasing rate leads to the refractive index crossover at around 300 °C.

Based on the measured refractive indices' crossover condition, we can easily eliminate the misleading scattering intensity data (in the transparent region) during the cloud point measurements at

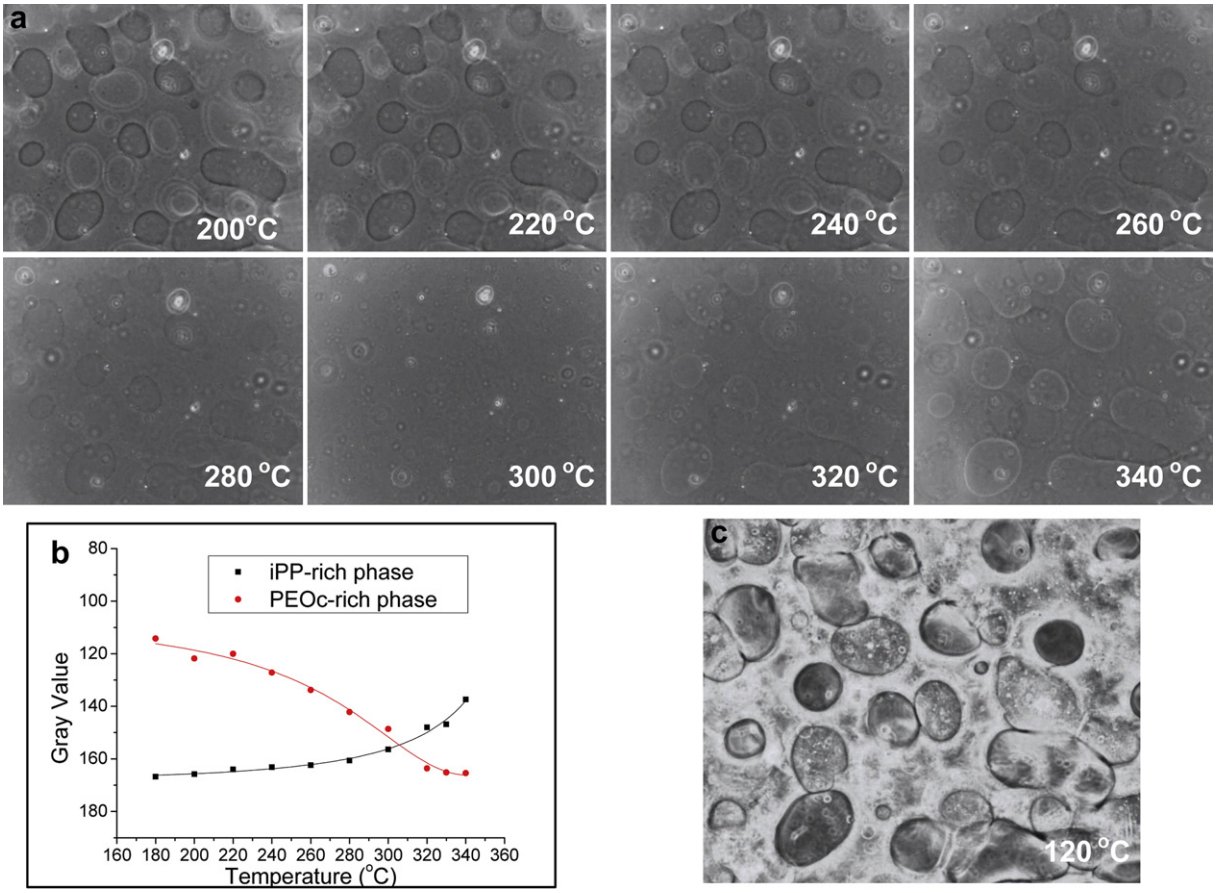

Fig. 2. (a) Temperature dependent inversion of two phases' contrast of W50.0's morphology. Sample was heated to the desired temperature at a rate of 30 °C/min and keep 1 min for phase contrast microscopy observation for every 20 °C. The width of the image is 450 μm. The PEOc-rich phase corresponded to the dark areas of the interconnected structure below 300 °C and corresponded to the bright areas above 300 °C. (b) Temperature dependence of gray intensity levels of each phases form the analysis of phase contrast micrographs showed in (a). (c) Corresponded crystallization morphology (cool to 120 °C at 30 °C/min), which further proved our assumption.

different cooling rate. Then, correct cloud points can be obtained for compositions under reasonable experiment temperatures (below 350 °C) to avoid any degradation or crosslink of polymers. These reasonable cloud points at extrapolated zero cooling rate can only be obtained at off-critical compositions (high iPP or high PEOc component) as shown in Fig. 4 because for middle concentrations the miscible region is higher than the temperature where experimental measurements are possible.

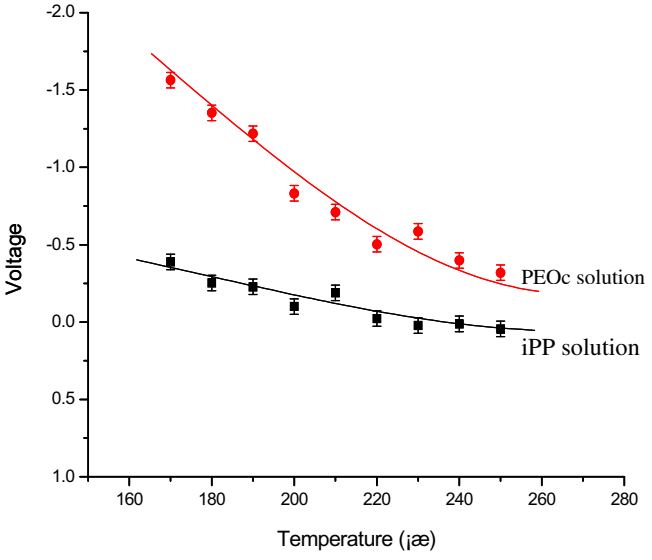

Fig. 3. Plots of voltage of the position-sensitive detector vs. temperature.

For binodal phase boundary of a strictly binary system, polymer 1 with chain length m_1 and polymer 2 with chain length m_2, the chemical potentials can be expressed [29] as following:

$$\frac{\Delta\mu_1}{m_1RT} = \frac{\ln\phi_1}{m_1} + \frac{1}{m_1} - \frac{\phi_1}{m_1} - \frac{\phi_2}{m_2} + \xi_1\phi_2^2 \tag{4}$$

$$\frac{\Delta\mu_2}{m_2RT} = \frac{\ln\phi_2}{m_2} + \frac{1}{m_2} - \frac{\phi_1}{m_1} - \frac{\phi_2}{m_2} + \xi_2\phi_1^2 \tag{5}$$

where $\xi_1 = g - \phi_1\,\partial g/\partial\phi_2$; $\xi_2 = g + \phi_2\,\partial g/\partial\phi_2$; ϕ_1, ϕ_2 is volume fraction of polymer 1 and polymer 2. R is the gas constant of 8.314 J/(mol K). T is the temperature. μ_1 and μ_2 are chemical potential of polymer 1 and polymer 2 respectively. ξ is the Flory–Huggins Interaction parameter.

At equilibrium between phase a and b we have.

$$\Delta\mu_{1a} = \Delta\mu_{1b}$$

$$\Delta\mu_{2a} = \Delta\mu_{2b}$$

So, $\Delta\mu_1 = 0$, and $\Delta\mu_2 = 0$

Generally the Flory–Huggins Interaction parameter ξ is written as χ, therefore we can obtain equations (6) and (7) from equations (4) and (5).

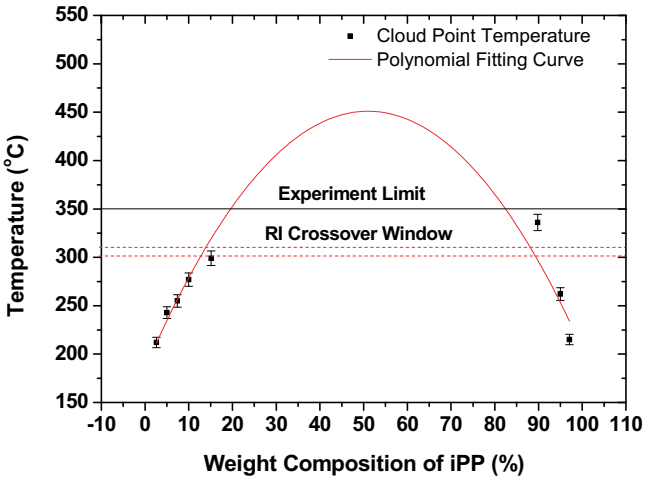

Fig. 4. Composition dependence of the cloud point and the fitting phase diagram. The transparent window was caused by the refractive indices inversion.

$$\frac{\Delta\mu_1}{m_1RT} = \frac{\ln\phi_1}{m_1} + \frac{1}{m_1} - \frac{\phi_1}{m_1} - \frac{\phi_2}{m_2} + \chi\phi_2^2 = 0 \quad (6)$$

$$\frac{\Delta\mu_2}{m_2RT} = \frac{\ln\phi_2}{m_2} + \frac{1}{m_2} - \frac{\phi_1}{m_1} - \frac{\phi_2}{m_2} + \chi\phi_1^2 = 0 \quad (7)$$

Since in the Flory–Huggins Lattice model, equal monomeric volume is used, therefore we will use iPP monomer as the reference in the calculation of phase chain length.

We knew that $M_{0(1)} = M_{0(\mathrm{iPP})} = 42$, and $M_{0(2)} = M_{0(\mathrm{PEOc})} = 112$.

And we also have $M_{w(1)} = M_{w(\mathrm{iPP})} = 41 \times 10^4$, and $M_{w(2)} = M_{w(\mathrm{PEOc})} = 15 \times 10^4$ from GPC test results.

If we assume iPP and PEOc have the same density, then specific volume should be proportional to monomeric molecular weight and, $m_1 = 41\times10^4/42 = 9.76\times10^3; m_2 = 15\times10^4/112\times112/42 = 3.57\times10^3$ if g is a simple function of temperature and composition, we may assume $g = a + b/(T\phi_1\phi_2)$. Where, a and b are parameters. Then we can obtain $\chi = g - \phi_1\frac{\partial g}{\partial\phi_2} = g + \phi_2\frac{\partial g}{\partial\phi_2}$.

We know χ is very small for iPP and PEOc and the resulting differential equation for cloud point temperature curve is a Transcendental Equation. It is very difficult to obtain an accurate solution from equation (6) and equation (7) because the fitting parameters are highly corrected.

Using the Taylor series expansions $\ln(1-x) = -(x + x^2/2 + x^3/3 + x^4/4 + \ldots\ldots)$ $(0 < x < 1)$, then fitting the quadratic equation (8), we can obtain a phase diagram as shown Fig. 4a.

$$T_{\text{cloud point}} = A + B\phi_2 + C\phi_2^2 \quad (8)$$

Where A, B, C, are fitting parameters. If we give the intercept value A as 185, then B, C will be 10.429 and −0.102 separately. The R residual square is 0.9953. This phase diagram can also be compared a published the simulation result [30]. Alternatively A, B and C can be obtained from the equation (8) if we assume a critical point ϕ_c and a critical temperature T_c. Since both cannot be measured in our current experimental system, we can only result to the above quadratic approximation.

4. Conclusion

The refractive indices of all polyolefin are very close to each other. For the iPP/PEOc blends used in this study, refractive indices inversion has happened in the temperature region around 306 °C. The refractive indices inversion phenomena could easily led to a mis-interpretation that there is an existence of a one phase region and a UCST and LCST duo phase separated regions below and above that temperature region. Measurements of DSC, phase contrast images at different temperatures, thermal history and kinetics, image analysis, cloud point, as well as the refractive index measurements of the blends and each polymer in solution have led to our conclusion and the constructed UCST phase diagram for the iPP/PEOc blend.

Acknowledgements

We would like to thank the generous financial support by following grants: National Natural Sciences Foundation of China, grant No. 50773087 and 20490220.

References

[1] Yano A, Akimoto A. Metallocene-catalysed polymers – materials, properties, processing and markets. Norwich, New York. In: Bendikt GM, Goodall BL, editors. Plastic design library; 1998. p. 98.
[2] Parikh DR, Edmonson MS, Smith BW, Winter JM, Castille MJ, Magee JM, et al. Metallocene-catalysed polymers – materials, properties, processing and markets. Norwich, New York. In: Bendikt GM, Goodall BL, editors. Plastic design library; 1998. p. 113.
[3] Utracki LA. Polymer alloys and blends: thermodynamics and rheology, vol. 20. New York: Hanser Publishers; 1989.
[4] Gupta AK, Ratnam BK, Srinivasan KR. J Appl Polym Sci 1992;45:1303.
[5] Wal A, Mulder JJ, Oderkerk J, Gaymans RJ. Polymer 1998;39:6781.
[6] Hornsby PR, Premphet K. J Appl Polym Sci 1998;70:587.
[7] Premphet K, Horanont P. Polymer 2000;41:9283.
[8] Jang BZ, Uhlmann DR, Vander Sande JB. J Appl Polym Sci 1984;29:4377.
[9] Yamaguchi M, Nitta KH, Miyata H, Masuda T. J Appl Polym Sci 1997;63:467.
[10] Krause S. Polymer–polymer compatibility. In: Paul DR, Seymour N, editors. Polymer blends, 1. New York: Academic Press; 1978. p. 15.
[11] Mehta R, Keawwattana W, Kyu T. J Chem Phys. 2004;120:4024.
[12] McNally T, McShane P, Nally GM, Murphy WR, Cook M, Miller A. Polymer 2002;43:3785.
[13] Da Silva Ana Lúcia N, Rocha Marisa CG, Coutinho Fernanda MB, Bretas Rosário, Scuracchio Carlos. J Appl Polym Sci 2000;75:692.
[14] Ryu DY, Lee DH, Jang J, Kim JK, Lavery KA, Russell TP. Macromolecules 2004;37:5851.
[15] Ryu DY, Park MS, Chae SH, Jang J, Kim JK, Russell TP. Macromolecules 2002;35:8676.
[16] Hu HQ, Cong CB, He AH, Zhang CG, Fan GQ, Dong JY, et al. Macromol Rapid Commun 2005;26:973.
[17] Wu C, Xia KQ. Rev Sci Instrum 1994;65:587.
[18] Han CC, Yao YH. China patent application. 2005; 200510123609.9.
[19] Flory PJ, Orwoll RA, Vrij A. J Am Chem Soc 1964;86:3507.
[20] Flory PJ, Orwoll RA, Vrij A. J Am Chem Soc 1964;86:3515.
[21] Flory PJ. J Am Chem Soc 1965;87:1833.
[22] Abe A, Flory PJ. J Am Chem Soc 1965;87:1838.
[23] Eichinger BE, Flory PJ. Trans Faraday Soc 1968;64:2035.
[24] de Gennes PG. J Chem Phys 1980;72:4756.
[25] de Gennes PG. Scaling concepts in polymer physics, vol. 98. New York: Cornell University Press; 1979.
[26] Siggia ED. Phys Rev A 1979;20:595.
[27] Sanchez IC, Balazs AC. Macromolecules 1989;22:2325.
[28] Fuller GG. Optical rheometry of complex fluids. New York: Oxford University Press; 1995.
[29] Koningsveld R, Stockmayer WH, Nies E. Polymer phase diagrams. New York: Oxford University Press; 2001. 234.
[30] Li ZW, Lu ZY, Sun ZY, Li ZS, An LJ. J Phys Chem B 2007;111:5934.